International Journal of Mechanical, Industrial and Aerospace Sciences
ISSN: 2517-9950
Vol:3, No:10, 2009

Air flow and heat transfer modeling of an Axial Flux Permanent Magnet Generator

Airoldi G.[1], Bumby J.R.[1], Dominy C.[1], G.L. Ingram[1], Lim C. H.[1], Mahkamov K.[1], N.L. Brown[2], A. Mebarki[2] and M. Shanel[2]

***Abstract*—**Axial Flux Permanent Magnet (AFPM) Machines require effective cooling due to their high power density. The detrimental effects of overheating such as degradation of the insulation materials, magnets demagnetization, and increase of Joule losses are well known. This paper describes the CFD simulations performed on a test rig model of an air cooled Axial Flux Permanent Magnet (AFPM) generator built at Durham University to identify the temperatures and heat transfer coefficient on the stator. The Reynolds Averaged Navier-Stokes and the Energy equations are solved and the flow pattern and heat transfer developing inside the machine are described. The Nusselt number on the stator surfaces has been found. The dependency of the heat transfer on the flow field is described and the stator temperature field obtained. Tests on an experimental rig are undergoing in order to validate the CFD results.

***Keywords*—**Axial Flux Permanent Magnet machines, Thermal Modeling, CFD.

I. Introduction

In order to build a detailed thermal network representing an electrical machine, the heat transfer coefficients on the surfaces of a generator are necessary to model the convective heat transfer. These can be obtained either through experiments or by numerical simulations. In this paper a 3D Computational Fluid Dynamics analysis of the experimental test rig built at Durham University is presented. The test rig is a scaled-up replica of an actual AFPM machine.

A previous study [1] on a simplified geometrical model to find the influence of parameters such as magnets' depth, running clearance, and rotational speed on the stator's heat transfer had been completed. Other studies ([2], [3] and [4]) have considered simplified models such as systems consisting of a rotor disc facing a stationary disc to understand flow and heat transfer patterns developing inside. Various configurations of rotor-stator layout have been considered by different authors. The one most relevant to the cooling of a stator of an AFPM machine consists of a rotor facing a heated stator with an opening which allows for cooling air inflow [5], [6]. The two types of flows occurring inside rotor-stator systems take their names from the first two researchers who first discovered them: Batchelor [10] and Stewartson [11]. The first consists of two boundary layers formed on the rotor and the stator respectively and separated by a rotating core of fluid, whereas the second one consists of a boundary layer on the rotor. Daily and Nece [8] identified 4 types of flows depending on the values of the non-dimensional air gap G and the peripheral Reynolds number which develop in rotor-stator systems:

1) Laminar boundary layers on both (rotor and stator) surfaces with the two BL covering the whole gap thickness (occurring at low air gap ratio $G=s/R_{out}$).
2) At high values of G there are two separated boundary layers: one on the rotor and one on the stator and they are separated by a rotating core.
3) Equivalent to regime 1, but with turbulent boundary layer.
4) Equivalent to regime 2, but with turbulent boundary layer.

In a more recent study [9] Poncet et Al. described the transition between a Batchelor type to a Stewartson type of flow. The studies in the available literature refer to models consisting of a flat rotor facing a flat stator and without any additional geometric feature.

In the present study a model of a complete AFPM generator is analyzed, Nusselt numbers on the stator's surfaces are found together with velocity and temperature field.

II. Model

The modeled machine consists of an annular stator, a stator holder and two rotors carrying each 16 sectors representing the magnets. The rotors and the magnets are made of Perspex. The rotors are held together by a boss consisting of aluminum prisms.

The air enters through a circular opening in the rotor disc, then it flows through the running clearance under the boss action and under the effect of the magnets (Fig. 1). The CFD model has been built by modeling all the rig components and the air inside it. An additional fluid domain has been added outside the generator due to the absence of an enclosure. Since the generator has a geometrical periodicity of 45°, only $1/8^{th}$ of it has been modeled and periodic boundary conditions have been applied to the matching faces. In Fig. 1 the periodicity of the test rig is shown by white lines which separate the generator into sectors. Since the test rig is a scaled up model of an actual machine, it is convenient to express the dimensions in non-dimensional terms. The most relevant non-dimensional quantities are shown in Table 1.

[1]School of Engineering, Durham University, Durham, DH1 3LE, UK
[2]Cummins Generator Technologies, Barnack Road, Stamford, Lincolnshire, PE9 2NB, UK
E-mail of Corresponding Author: giovanni.airoldi@durham.ac.uk
Telephone: +44 0191 3342509).

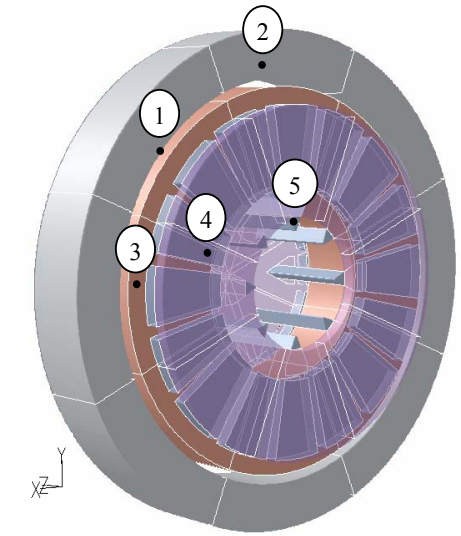

Fig. 1 AFPM machine test rig: (1) Stator, (2) Stator holder, (3) Magnets, (4) Rotor, (5) Boss. The periodic division is shown on the 3D drawing. A cross section along the zy plane displays the inlet and the outlet regions.

TABLE I
NON-DIMENSIONAL QUANTITIES

Symbol	Quantity	Definition	Value
G	Non-dimensional running clearance	s/R_{out}	0.02
M	Non-dimensional magnet depth	m/R_{out}	0.075
D	Non-dimensional inlet diameter	d/R_{out}	0.375
Re_{out}	Peripheral Reynolds number	$(\rho\Omega R_{out}^2)/\mu$	855,000

The mesh consists of 8 million hexahedral elements (Fig. 2). The picture shows the inlet, outlet, and periodic boundaries. The commercial package Fluent has been used to solve the steady state Reynolds Averaged Navier Stokes equations. The realizable κ-ε model has been chosen for the closure of the system of equations. Two approaches are available in Fluent to model the near-wall regions. The first one relies on wall functions and the second one is the so called Enhanced Wall Treatment which corresponds to a 2 layer approach. In this study the latter has been chosen to model the walls. The mesh has been generated accordingly to this method and satisfies the requirement of $y^+\sim1$ [7] on all the walls of the domain. This has required generating a mesh which features 23 elements in the running clearance between stator and magnets. Previous studies carried out on a system with equivalent Reynolds number Re_{out} have also shown that this number of elements guarantees a mesh independent solution. A further mesh refinement would unnecessarily increase the computational time. Two criteria had to be satisfied for convergence: the residuals relevant to the flow quantities had to be in the order of 10^{-3}, the energy residual in the order of 10^{-6}, and the monitored velocity components in the air gap had to be independent of the number of iterations. The residuals were well below the requirements (in the order of 10^{-5} for the velocity components and turbulent quantities and in the order of 10^{-8} for the energy equation) when the convergence was reached.

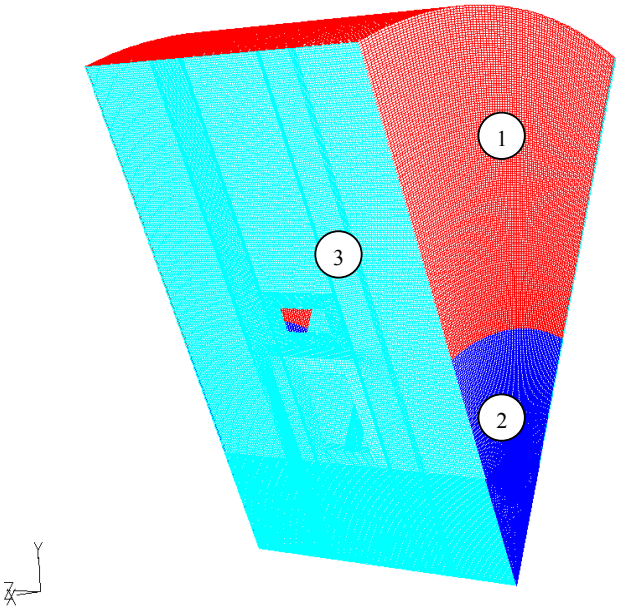

Fig. 2: Mesh regions: 1) Outlet, 2) Inlet, 3) Periodic boundary. The boundary conditions are represented in Table 2.

TABLE II
BOUNDARY CONDITIONS

Quantity	Symbol	Value
Inlet pressure	P_{tot} (Pa)	0
Outlet pressure	P_{st} (Pa)	0
Inlet temperature	T_{in} (K)	293
Stator inner wall heat flux	Q (W/m^2)	1000

The analysis has been conducted by solving the time averaged continuity equation, the momentum equation, and the turbulent model equation. The Multiple Reference Frame (MRF) method has been used in Fluent in order to take account of the rotation of the generator's components and of the cooling air. Since the temperature gradients inside the domain is not significant, the air density has been considered independent of the temperature. This corresponds to considering the dynamic effects preponderant on the buoyancy ones. A vertical section (zy plane) of the machine is displayed (Fig. 3) to highlight the air flow.

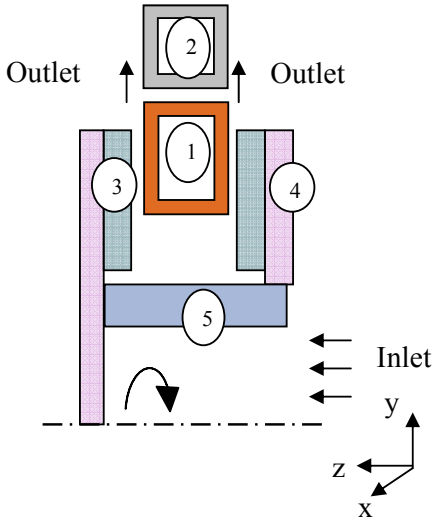

Fig. 3: zy plane cross section of the machine: (1) Stator, (2) Stator holder, (3) Magnets, (4) Rotor, (5) Boss.

III. Results

The velocity contours obtained at two angular positions (on the vertical plane, and on an inclined plane crossing the groove between magnets) show that most of the air flow occurs between the magnets (Fig. 4a and Fig.4b). The velocity contours on the whole domain (including the test rig and the additional domain outside it) are displayed. The radial velocity in the running clearance on the vertical plane was obtained at 4 radii (Fig. 5) The flow is outward in the whole running clearance until r/R_{out} =0.86 where some reversed from starts appearing on the stator side. The turbulent nature of the flow is evident from the flat radial velocity profile especially at r/R_{out}=0.57.

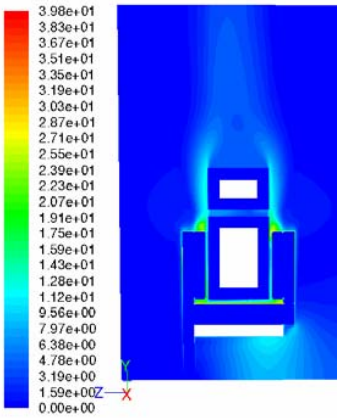

Fig. 4a: Velocity contours on a plane crossing a magnet.

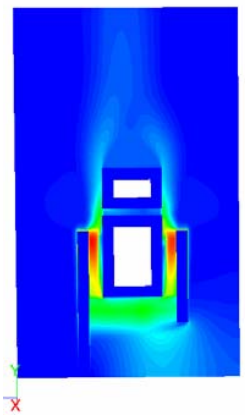

Fig. 4b: Velocity contours on a plane crossing a groove between the magnets.

Whereas for $r/R_{out} \geq 0.57$ a constant tangential velocity can be seen across the running clearance (Fig. 6), at the running clearance inlet (r/R_{out}=0.5), the tangential velocity progressively changes from a maximum on the rotor to zero on the stator surface.

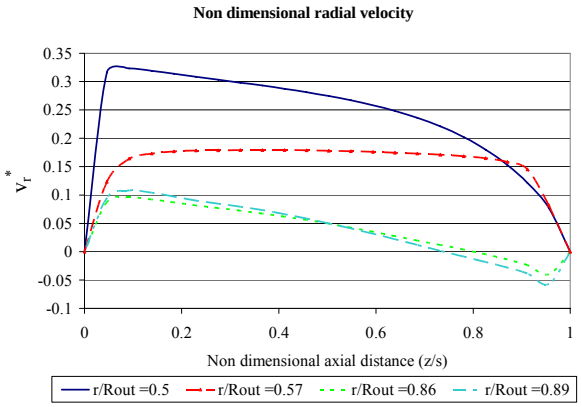

Fig. 5:Non-dimensional radial velocity in the running clearance.

Due to the absence of an enclosure, most of the fluid domain is at room temperature. The stator inner surface benefits from both low temperature and high velocity of the incoming air from the boss (Fig. 7). The highest temperature region is the one under the stator holder. The stator surface temperature is quite uniform (within 1°C temperature gradient), but a higher temperature in the center of the surface facing the rotor can be observed. This high temperature coincides with the low heat transfer coefficient at the same location (Fig. 8).

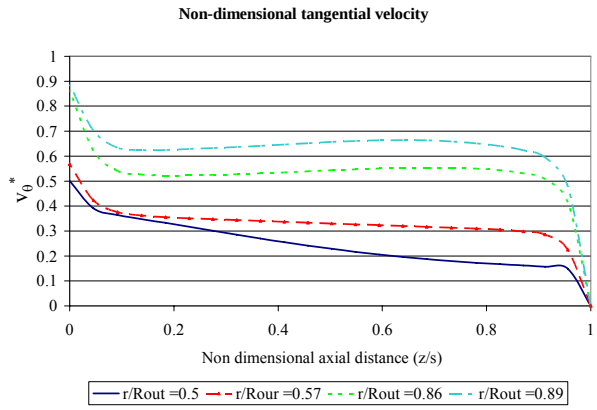

Fig. 6: Non-dimensional tangential velocity in the running clearance.

The heat transfer coefficient has been calculated by using the air inlet temperature as a reference. The heat transfer coefficient (Fig. 8) is high at the running clearance inlet where the radial velocity is high because of lowest passage area, then it decreases at the mid radius and increases again at the periphery due to the increase of tangential velocity. The heat transfer coefficient therefore depends on the velocity magnitude in the running clearance. The drop in heat transfer coefficient at the outer radius is due to the reversed flow occurring in the vicinity of the stator surface.

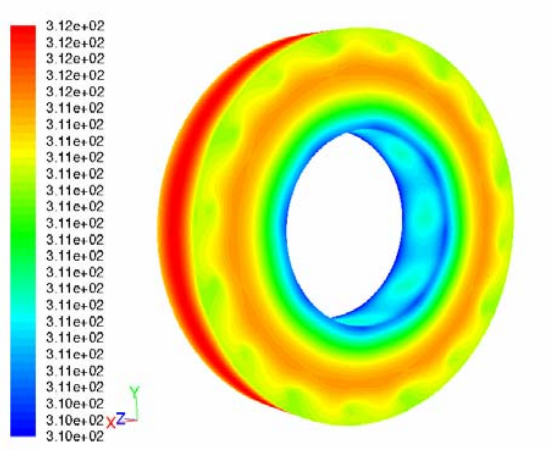

Fig. 7: Stator temperature contours (K)

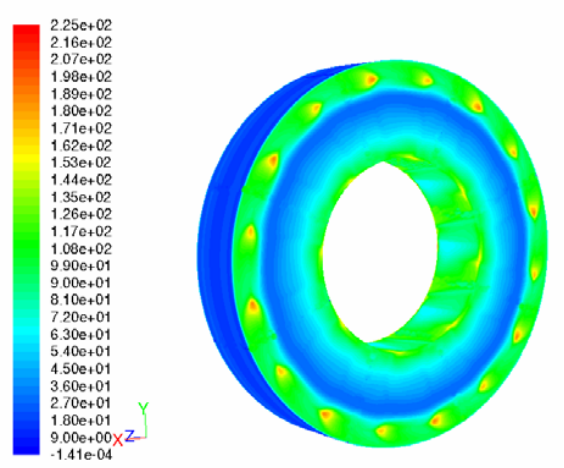

Fig. 8: Stator heat transfer coefficient contours (W/(m^{2}K))

It is convenient, in order to have general results applicable to similar systems, to the one here analyzed, to calculate the Nusselt number on the stator annular surface facing the rotor. This is done by using the local radius as characteristic length:

$$Nu(r) = \frac{h(r)r}{k} \quad (1)$$

In Fig. 9 the angular locations where the local Nusselt number has been calculated are shown.

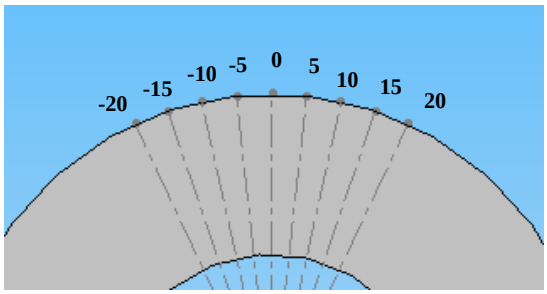

Fig. 9: Angular location of Nusselt number on the stator annular surface.

The Nusselt number is independent on the angular location for most of the radial extension of the running clearance (Fig. 10). The non dimensional radial coordinate r/R is calculated using the stator outer radius R. Since the rotor's radius is smaller than the stator's, the outer boundary of the running clearance coincide with (r/R=0.9). The Nu numbers at the various angles are mostly uniform in the running clearance whereas a difference can be noticed for r/R>0.9 with the maximum Nu obtained at -16°.

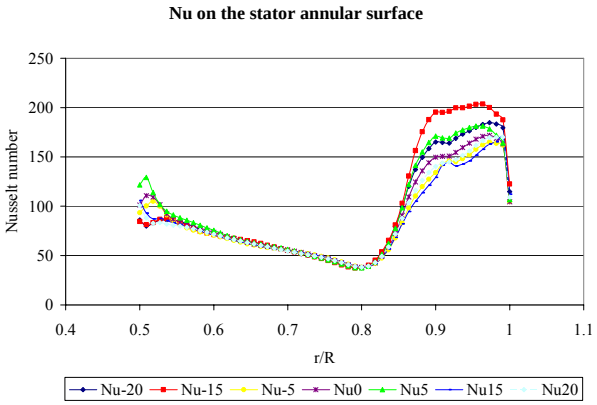

Fig. 10: Stator annular surface Nusselt number.

The Nusselt number on the inner and outer cylindrical surfaces of the stator has been calculated along the axial coordinate by using the cylinder radius as characteristic length: the stator inner radius R_i for the inner cylinder and the stator outer radius R for the outer one (Fig. 11). Due to the symmetry with respect to the mid xy plane, the graph in Fig. 11 only shows the Nusselt number from the centre of the stator to the periphery. The high velocities caused by the rotating boss at the inner radius are responsible for the high Nu number there. At the outer stator radius Nu is considerably lower due to the absence of the effects from the boss and due to the stator holder which reduces the velocity magnitudes.

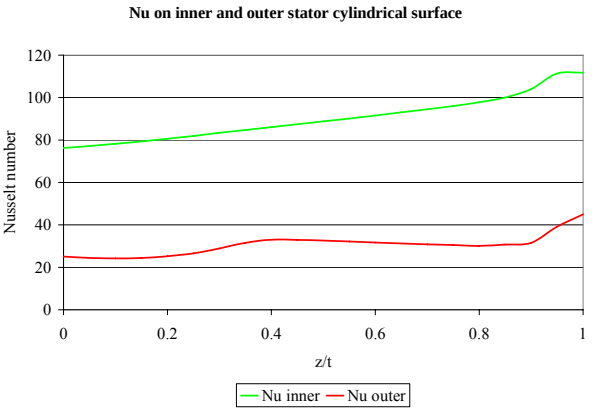

Fig. 11: Stator top and bottom cylindrical surface Nusselt number

IV. CONCLUSIONS

A CFD simulation on a model of an AFPM machine has

been conducted. The flow pattern and the heat transfer from the stator have been described.

The analysis of the velocities in the running clearance demonstrates that a rotating core exists at the periphery, whereas at the inlet the tangential velocity progressively varies from its maximum value on the rotor to become zero on the stator.

The Nusselt number on the stator has been obtained and its pattern follows the velocity magnitude in the running clearance.

The beneficial effect of the boss is evident as it leads to a high heat transfer and to low temperature of the stator inner cylindrical surface.

TABLE III
NOMENCLATURE

Symbol	Quantity	
d	Inlet rotor diameter	(m)
$h(r)$	Stator local heat transfer coefficient	$W/(m^2K)$
m	Magnet depth	(m)
$Nu(r)$	Local Nusselt number	
P_{st}	Static pressure	(Pa)
P_{tot}	Total pressure	(Pa)
Q	Stator heat flux	(W/m^2)
r	Stator local radius	(m)
R	Stator outer radius	(m)
R_i	Stator inner radius	(m)
R_{out}	Rotor outer radius	(m)
s	Running clearance	(m)
t	Stator axial thickness	(m)
T_{in}	Air inlet temperature	(K)
v_θ	Tangential velocity	*(m/s)*
v_r	Radial velocity	*(m/s)*
v_θ^*	Non-dimensional tangential velocity	$v_\theta^* = v_\theta/(\Omega R_{out})$
v_r^*	Non-dimensional radial velocity	$v_r^* = v_r/(\Omega R_{out})$
k	Air conductivity	(W/(mK))
μ	Air viscosity	(Pa·s)
Ω	Angular speed	(rad/s)
ρ	Air density	(kg/m^3)

REFERENCES

[1] G. Airoldi, G.L. Ingram, K. Mahkamov, J.R. Bumby, R.G. Dominy, N.L. Brown, A. Mebarki and M. Shanel "Computations on Heat Transfer in Axial Flux Permanent Magnet Machines" IEEE Proceedings of the 2008 International Conference on Electrical Machines.

[2] J. Pelle' and S. Harmand "Heat transfer measurements in an opened rotor-stator system air-gap", Experimental Thermal and Fluid Science, (2007), pp 165-180.

[3] Z. X. Yuan, N. Saniei and X. T. Yan, "Turbulent heat transfer on the stationary disk in a rotor-stator system", International Journal of Heat and Mass Transfer, (2003), pp 2207-2218.

[4] S. Harmand, B. Watel, B. Desmet, "Local convective heat exchanges from a rotor facing a stator" Int. J. Therm. Sci, (2000), pp 404-413.

[5] R. Boutarfa, S. Harmand, "Local convective heat exchanges and flow structure in a rotor-stator system", Int. J. Therm. Sci. (2003), pp 1129-1143.

[6] J. Pelle' and S. Harmand, "Heat transfer study in a rotor-stator system air-gap with an axial inflow", Applied hermal Engineering, (2009), pp 1532-1543.

[7] Fluent.Inc. "Computational Fluid Dynamic Software", User's guide release 6.3, Lebanon, NH, USA, 2006

[8] J. W. Daily, R. E. Nece, "Chamber dimension effects on induced flow and frictional resistance of enclosed rotating disks", Transactions of the ASME. Series D, Journal of Basic Engineering, (1960), pp 217-232.

[9] S. Poncet, M. P. Chauve and R. Schiestel, "Batchelor versus Stewartson flow structures in a rotor-stator cavity with throughflow", Physics of fluids, (2005).

[10] G. K. Batchelor, "Note on a class of solutions of the Navier-Stokes equations representing steady rotationally-symmetric flow", Q. J. Mechanics Appl. Math, Vol. 4, (1951), pp 29-41.

[11] Stewartson, K., "On the flow between two rotating coaxial disks", Mathematical Proceedings of the Cambridge Philosophical Society, (1953) pp 333-341.